EXPERIMENTAL EVALUATION OF THE SEISMIC PERFORMANCE OF MODULAR STEEL BRACED FRAMES

C.D. Annan, M.A. Youssef[1], M.H. El Naggar
Department of Civil and Environmental Engineering, The University of Western Ontario, London, ON, N6A 5B9. CANADA

Abstract

Several studies have shown that the lateral response of concentrically braced frames is dominated by the inelastic behavior of the bracing members. However, the overall performance of the entire frame depends on the frame configuration including its connections. In this study, the hysteretic characteristics of modular steel braced frames under reversed cyclic loading are evaluated. The design and construction of the test specimen accounted for the unique detailing requirements of these frames. A regular concentrically braced frame with similar physical characteristics was also tested for comparison. Both test specimens consisted of a one-storey X-braced system with tubular brace cross-section. This paper describes the behavior characteristics and provides a detailed comparison of the two systems to assess the strength, stiffness, inelastic force and deformation, and energy dissipation characteristics of the modular system. An analytical model capable of capturing the effect of the system's unique detailing requirements is proposed and validated using the test results.

Keywords: Modular steel braced frame, experimental behavior, hysteretic behavior, strength, stiffness, energy dissipation, analytical modeling.

[1] Corresponding author. Tel.: +1 519 661-2111 Ext. 88661; Fax: +1 519 661-3779.
E-mail address: youssef@uwo.ca (M.A. Youssef)

1.0 Introduction

In spite of the increasing use of concentrically braced frames as an earthquake-load resisting system, there has been a growing concern related to their ultimate deformation capacity because of observed damages in past earthquakes. For example, concentrically braced frames were damaged during the 1985 Mexico earthquake [1], 1994 Northridge earthquake [2], and 1995 Hyogo-ken Nanbu earthquake [3]. The main source of energy dissipation in these frames is through inelastic deformation of bracing members. Seismic response of such frames is therefore dominated by the inelastic behavior of the bracing members.

Bracing members in frames of regular buildings are expected to buckle in compression and yield in tension when subjected to reversed cyclic loading. Plastic hinges often form after brace buckling. This may cause permanent plastic deformations and deterioration of the resistance in the braces. To promote ductile response, bracing connections are designed to tolerate the large rotations associated with brace buckling. They must also support the full tensile and compressive capacity of the brace during cyclic inelastic deformation demands. This implies that the connection cannot buckle or fracture prior to the development of the full resistance and ductility of the brace.

Several studies have revealed the complexity of the hysteretic behavior of steel braced frames [4], [5], [6], and [7]. This is due to significant degradation of strength and stiffness of braces in compression after a few post-buckling cycles. These studies further revealed that the main parameters that control this behavior are the width-to-thickness (w/t) ratio and the effective slenderness ratio (KL/r), where K is the effective length factor, L is the length of bracing member, and r is the radius of gyration. These observations have

caused considerable revision to design requirements of earthquake resistant steel braced frame structures [8] and [9]. These design codes now specify maximum design limits on KL/r and w/t to provide sufficient energy dissipation capacity and resistance to local buckling, respectively. In addition, the post-buckling phenomenon has been reasonably captured by applying a buckling reduction factor to the compressive strength of bracing members.

The complete hysteretic response of any framed structure, however, depends to a large extent on the overall frame configuration including its connection type. Modular steel buildings (MSBs) are being used increasingly for two to six storey schools, apartments, dormitories, hotels and in similar buildings where repetitive units are required. The lateral resistance of this unique building type is often achieved by adding diagonal braces. The characteristics and unique detailing requirements of MSBs have been described extensively by Annan et al. [10], [11], [12] and [13].

In MSBs, modular units made of high strength and durable steel sections are built and finished under a controlled manufacturing environment and are transported to the building site and connected horizontally and vertically. Lateral loading on each floor is transferred through the Horizontal Connections (HC) to the modular braced frame and then through the Vertical Connections (VC) to the foundation. Fig. 1 shows a typical plan and sections of a modular steel building. The following features specifically distinguish the MSB braced frame from a regular steel braced frame: (1) the existence of Ceiling Beams (CB) and Ceiling Stringers (CS) in the MSB frame system may result in natural periods and mode shapes different from those of conventional systems, (2) the Floor Beams (FB) may be set directly above the Ceiling Beams (CB) without mechanical connections except at

column locations, and this may result in structural contact interaction between the beam members, (3) the brace members in a typical modular steel frame do not intersect at a single working point which may lead to high seismic demands on the Vertical Connection (VC) between different units/modules, (4) the Horizontal Connections (HC) of separately finished modules, shown in section A-A, are achieved by field-bolting of clip angles which are shop-welded to the floor beams; (5) the vertical connection (VC) between modular units, shown in section B-B, typically involves partial welding of the columns of a lower and an upper modules which may lead to independent upper and lower rotations at the same joint. Column continuity is known to contribute effectively in preventing soft-storey response in multi-storey structures. Discontinuity of columns coupled with a possible high seismic demand on the vertical connection of different modules may result in a concentration of inelasticity in one storey over the height of the frame.

Currently, conventional design methods are followed in the seismic design of MSBs. There have been no previous studies to predict their behavior. Consequently, there are no guidelines to help engineers correctly assess their stiffness, strength, ductility, and cumulative hysteretic energy dissipation capacity. This paper introduces the first experimental investigation of the behavior of MSB braced frames under repeated cyclic loading. The study takes into account their unique detailing requirements. The paper describes the selection of specimen configuration and its design, experimental set-up, testing protocol, and results of the cyclic testing of a MSB braced specimen and a regular braced specimen. Experimental results are also compared to numerical predictions to validate the proposed modeling technique.

2.0 Selection of Specimen Configuration and Design

The experimental program involved testing two specimens: one MSB braced frame and one regular braced frame. The MSB braced specimen is a one-storey, one-bay cross-braced panel extracted and scaled from a typical four-storey modular building frame, shown in Fig. 2. This frame was designed according to the requirements of the Canadian standard CSA-S16.1 [8] and the National Building Code of Canada [14]. The MSB specimen consists of two columns, two cross bracing members, a floor beam and a ceiling beam of a lower modular unit, and a floor beam of a fictitious upper modular unit. A clearance of 40 mm was allowed between the bottom flange of the floor beam and the top flange of the ceiling beam to allow for a fire protective layer to be installed, as in current practice. The specimen was scaled at 3/8 of the full-scale size to be as large as possible considering the constraints of the available equipment (i.e. capacity of actuator) and supporting structures (i.e. location of hold-down bolts for the supporting frame) in the structural engineering laboratory at the University of Western Ontario. The MSB specimen was designed using forces scaled from those developed in the full-scale panel design such that stress conditions would remain similar in the two panels.

The regular braced specimen is a one-storey, one-bay cross-braced frame and was selected to have similar physical characteristics as the MSB specimen for effective comparison (i.e. same clear height, width and member proportions). This specimen consists of two columns, two cross bracing members, and top and bottom floor beams connected to the columns.

The dimensions of the two frame specimens are shown in Fig. 3. Detailing of the specimens was done in accordance with current professional practice. Fig. 4 shows photos

of specific details in the two test specimens. For the MSB specimen, beam-to-column connections were achieved by direct welding of the members, as shown in Fig. 4a. The upper brace ends were connected through gusset plates to the ceiling beam and columns which form part of the lower modular unit. The lower brace ends were connected through gusset plates to the floor beam and columns of the same unit. The two columns of this unit were connected to the floor beam of the fictitious upper unit by welding column cap plates to the lower flange of the beam, as shown in Fig. 4a. This welding was achieved only at the three exterior faces/sides, at each end of the specimen, which were accessible. In the regular braced specimen, beam-to-column connections were achieved by welding a plate to both the beam and column allowing for partial rotation between adjoining members, as shown in Fig. 4b.

The design yielded a HSS 32x32x3, imperial designation HSS 1 ¼ x 1 ¼ x .125, hollow tube sections (outside dimensions of 32 mm and a wall thickness of 3.2 mm) for the braces. Following capacity design procedures, the load capacity of this brace section was used to size the beams and columns so they would be able to resist induced forces when braces reached their yield strength. All beams (ceiling and floor) were made of W100x19 sections, imperial designation W4x13, and the columns were fabricated from a HSS 51x51x5, imperial designation HSS 2x2x.188, tube sections (outside dimensions of 51 mm and a wall thickness of 4.8 mm). The brace end connections were designed to remain elastic at all times so they would be at least as strong as the bracing member. This design maximized the energy dissipation capacity of the specimens. Single gusset plates of 8 mm thickness were selected for the brace end connections to the beams and columns. The tube brace members were slotted at each end and fillet welded to the gusset plates, as shown in

Fig. 4a. The gusset plates were designed with a free length of twice the gusset plate thickness to allow for rotation of the brace ends as recommended in the AISC design provisions [9] and used by Yoo et al. [15]. The plates were designed to possess sufficient tension and buckling capacities. They were welded to the beams and columns, as shown in Fig. 4a. The brace intersection point was achieved by cutting a slot through one brace member and welding a 10 mm thick connecting plate to this member and to the other crossing brace member, as shown in Fig. 4c. The plate was designed to carry the full tensile yield resistance of the bracing members and welded to develop continuity. For the MSB specimen, the welded connections between the column cap plates and the lower flange of the floor beam was designed based on the yielding capacity of bracing members, assuming equal distribution of forces at the ends of the specimen.

The selected boundary conditions for the specimens simulated those of the full-scale panels. Two 19 mm diameter bolts, with a total factored tensile resistance of 236 kN and separated by 152 mm on center, were used to connect each column base plate to the reaction frame (Fig. 4d). Prying action was accounted for in the design of these base plates. This provided the basis for selecting a 20 mm thick plate. Typical 5 mm circumferential fillet welds were used to connect the columns to the base and cap plates.

3.0 Experimental Setup

The test setup was chosen to adequately simulate all important field and boundary conditions. The specimens were mounted as shown in the photos of Fig. 5. Fig. 6 shows a schematic representation of the setup. The specimens were rotated at an angle of 90 degrees, making their columns align horizontally and the beams vertically. The load and

displacement actuator, with a maximum load capacity of 250 kN and a maximum movement of 45 mm, was thus mounted in a vertical position to provide the “lateral” cyclic loading / displacement to the test specimens at the level of “upper” floor beams. The specimens were connected to the actuator by means of a 25.4 mm thick plate welded to one end of top floor beam and bolted to a plate-tube welded assembly which is attached to the load actuator by a pin. They were braced as shown in Fig. 5 to prevent any out-of-plane movement or twisting of specimens during loading. The specimens were connected to the reaction frame by bolting of base plates of the two tube columns. The effect of gravity loading on the stability of restoring force characteristics of the test specimens was not simulated as it was considered to have no detrimental effect on the performance of the frames. Moreover, the gravity loading was considered not to follow a well established pattern that is applicable to all possible configurations.

The drift behavior of the test specimens was studied to allow an assessment of their ductility. The applied load and specimen drift were monitored at the top floor beam levels by the actuator. A total of 50 strain gauges and 7 LVDTs were installed at several locations on members of each specimen to measure strains and deformations. These readings were used to study the distribution of forces in the various members and at different sections of the specimens. Out-of-plane deformations of brace members were measured with LVDTs that were installed at ¼, ½, and ¾ times the distance between the free length regions of the gusset plates (labeled a, b, c, d, and e in Fig. 6). Four strain gauges were attached at each selected section to measure bi-axial bending stress and longitudinal stress. For the brace members; the strain gauges were installed at a number of locations along their longitudinal

direction (labeled a, b, c, d, and e in Fig. 6). All the instrumentations were plugged into a computerized data logger.

4.0 Experimental Program

The experimental program involved material testing, analytical predictions, and testing protocols.

4.1 Material Properties

Before the testing of the specimens, material testing was conducted to determine the basic monotonic steel stress-strain properties. The test procedure followed the ASTM standard test methods [16]. Standard coupon tests were conducted on six specimens of the bracing material to obtain an average yield stress of the tube brace section. There was no definite yield plateau for each of the specimens tested. The yield strength, F_y, was thus calculated using the 0.2% strain offset method. The average value for F_y was found to be 480 MPa with a standard deviation of 7.1MPa. The column tube section was not tested as it was delivered from the same consignment. Coupon tests were not performed for the beam sections as the beams were expected to remain elastic.

4.2 Pushover Analysis

Analytical prediction of the behavior of each frame specimen was carried out to develop suitable loading history, evaluate need for instrumentation and to avoid unexpected behavior during testing. Material data obtained from the coupon tests was used to conduct

nonlinear static pushover analyses of the specimens to predict their base shear- top displacement behavior.

Two-dimensional models were developed based on centerline dimensions of the specimens using the nonlinear computer program, SeismoStruct. A bilinear material model for steel was employed, with a kinematic strain hardening parameter of 2%. Inelastic beam-column frame element, which employs a cubic shape function [17], was used to represent the behavior of all frame members. This element type accounts for both geometric and material non-linearities. The element formulation is based on the fibre modeling approach that models the spread of material inelasticity along the member length and across the section area to allow for accurate estimation of structural damage distribution. In such elements, the sectional stress-strain state is obtained through the integration of the nonlinear uniaxial stress-strain response of the individual fibres in which the section has been subdivided. For the frame members, 200 section fibres were employed. The element response (curvatures and stress/strain peak values) is assembled from contributions at two gauss points, where the cross sections can be discretised into a number of monitoring points.

A joint element with uncoupled axial, shear and moment actions was utilised to allow rotation at the ends of bracing members. All beam-column joints in the MSB specimen model were assumed rigid to represent the directly welded connection between these members.

Fig. 7 shows a schematic representation of a proposed analytical model of vertical connection between columns of a lower unit and the top floor beam (or columns) of an upper unit. Rigid end blocks (shown by thick dark lines J1-J2, J3-J4, J5-J4, and J6-J4) were

provided at each end of frame members to capture the rigidity of connection regions. The short column segment between the bottom flange of the floor beam and top flange of the ceiling beam was represented by a vertical beam-column element, M1, whose height represents the clearance between the two beams. This vertical element was pinned internally into a common joint with the bottom flange of the floor beam, J2, such that an independent upper and lower module rotation would develop at this joint. Joints J3 to J6 are modeled as continuous.

The characteristic reduction in strength of a brace member after buckling was incorporated in the model by assuming an elasto-plastic brace behavior for the compression brace with the yield force taken as the residual strength after buckling [8], [18], and [19].

The analytical models of the test specimens were subjected to response control nonlinear pushover analyses. The magnitude of lateral forces, with a distribution pattern along specimens' height similar to the actual tests loading, was gradually increased up to a deformation similar to the expected actuator deformation capacity. A total of 250 incremental steps to the target displacement were applied.

Fig. 8 shows the base shear versus specimen displacement curves. The analytical yield strength, P_y, were estimated as 97.5 kN and 82.5 kN for the MSB and regular braced specimens, respectively. The yield strength was estimated by idealising the actual structural response curve by a bilinearly elasto-plastic curve such that the two curves yield the same total energy dissipation up to the point of ultimate deformation. The stiffnesses corresponding to the elastic portion of the load-displacement response were estimated as 17.2 kN/mm and 19.1 kN/mm for the MSB and regular braced specimens, respectively.

4.3 Testing Protocol

Testing of the frame specimens followed the Applied Technology Council's ATC-24 [20] single specimen testing program. The test specimens were subjected to symmetric reversed-cyclic loading histories to characterize their performance. Loading imposed by the actuator was done at a sufficiently slow rate (an average of 3.5 – 4.0 kN/sec in the elastic load cycles and 1.8 – 2.2 mm/sec in the inelastic load cycles) to prevent the development of any dynamic effects. In both loading and unloading branches of an excursion, loading was applied continuously without intermittent stops in order to reduce any strain rate effects. The yield values of specimen forces from the analytical study were used to initially control the test. Beyond the elastic range, the experimentally obtained values of the yield displacements were used as test control parameters.

Figs. 9 and 10 summarize the loading histories for both elastic (force-controlled) and inelastic (displacement-controlled) cycles applied to the two specimens, respectively. Three complete cycles at two load levels in the analytical elastic range ($0.33P_y$ and $0.67P_y$) were first applied to the specimens. Three cycles at the analytical yield load level, P_y, were then applied, noting any sign of visible nonlinearity in the force-displacement curve. The displacement corresponding to this point was taken as the actual yield displacement, Δ_y, and used to control subsequent loading cycles. Full cycles (3 or 2) at a constant peak deformation increment equal to twice the yield displacement were applied until significant strength deterioration was observed or the maximum actuator movement or capacity was reached. In the case of the latter, the specimen was cycled at the maximum peak deformation until severe deterioration was evident. Table 1 shows the load steps and cycles, and the displacement ductility levels reached for both test specimens.

5.0 Experimental Results

The experimental results reveal some similarities as well as significant differences in the cyclic response of the MSB and regular braced specimens. The following sections describe these behavioral characteristics.

5.1 Overall Hysteretic Behavior

Fig. 11 shows the base shear versus peak drift hysteresis obtained for the two specimens. Both test specimens showed ductile behavior and are stable up to large drift levels, although some degree of pinching is apparent in the hysteretic loops, especially for the regular specimen. Clearly, both specimens exhibited almost linear elastic response upon applying the first two load steps (i.e. six cycles of loading) in spite of possible existence of initial imperfections. The initial stiffnesses of the load-displacement curves were evaluated as 14.3 kN/mm and 15.5 kN/mm for the MSB and regular braced specimens, respectively. Within the third load step, significant nonlinearity was observed mid-way in the load-displacement curve for each specimen (as shown by the displacement ductility levels at this load step in Table 1). The movements in the actuator corresponding to this point were found to be about 4.5 mm and 3.8 mm for the MSB and regular braced specimens, respectively. These displacements correspond to a 0.35% and 0.34% drift, respectively. Strain gauge data obtained from the various members indicated that, in the regular braced specimen, buckling of compression brace resulted in the first significant sign of nonlinear behavior, while in the MSB specimen, flexural response due to column yielding caused initial nonlinearity.

The MSB specimen was tested successfully to a 3.5% drift, corresponding to ten times the yield displacement, Δ_y, and a base shear of 225 kN. This level of loading resulted in a significant bending deformation in the column segment between the bottom flange of the upper floor beam and the top flange of the ceiling beam, as shown in Fig. 12a. The test was terminated at this high ductility level. Prior to the end of the test, a maximum out-of-plane deformation of 2.2% of the brace length was measured at the mid-section of a lower half side of a brace member (labeled "b" in Fig. 6). The ratio of the maximum attained base shear to the yield base shear was evaluated as 3.5.

The regular braced specimen was successfully tested to 3.1% drift at displacement ductility of 9. The maximum base shear at this drift level was found to be 245 kN, which was about the maximum load capacity of the actuator. At this load step, significant out-of-plane deformation was observed at mid-section of the lower half of the brace member labeled "b" in Fig. 6. The specimen was further subjected to 20 cycles at 3.05% drift during which the brace member lower half suffered severe out-of-plane buckling, as shown in Fig. 12b. Maximum out-of-plane deformation of 4.0% of the total length of brace member was measured at this point. The level of ductility reached was deemed sufficient to terminate the test. The ratio of the maximum base shear to the yield base shear was evaluated as 4.2.

Strain gauges installed on the floor and ceiling beams showed that these members remained elastic throughout the different loading phases of the specimens as anticipated from the design. A maximum strain of 0.84% (8400 micro strain) was reached at the mid-section of the lower half of a tube brace member of the MSB specimen at 3.5% drift level. At the upper end section of the same brace member, maximum strain of 0.23% (2300 micro strain) was recorded at this stage of loading. At 2.8% drift, maximum strain of 0.33% was

recorded at the mid-section of the lower half of the brace member. For the regular braced specimen, strain of 0.35% was reached at the mid-section of the lower half side of a brace member at 2.8% drift. At 3.1% drift, maximum strain of 0.73% was recorded at the same section. Upon a number of repeated cycling at load step 8, brace members in this specimen reached maximum strain of 2.9% before the test was terminated.

5.2 Strength and Stiffness Characteristics of Specimens

As indicated in the previous section, the regular braced specimen showed greater initial lateral stiffness than the MSB braced specimen (i.e. initial lateral stiffness of MSB specimen was about 93% that of the regular specimen). This is because the regular braced specimen has greater lateral resistance provided by the truss action typical of concentrically braced frames. The MSB specimen in this range derived its lateral resistance from a combination of the brace action and some moment resisting action due to direct welding of members and moment connection between the column and the bottom flange of the upper floor beam.

The hystereses for the two specimens are fairly symmetrical in both the elastic and inelastic cycles. Both specimens showed stable behavior in almost every step of repeated loading. Fig. 13 shows the change in lateral stiffness with specimen peak drift and with maximum displacement ductility (i.e. ratio of peak deformation to actual yield deformation). Within the elastic response range, the lateral stiffness was evaluated as the slope of the base shear versus displacement relationships. Beyond this range, it was estimated as the slope of the line joining the peaks of positive and negative drifts in each remaining load step. Up to a ductility level of 2, the MSB braced specimen provided less

lateral stiffness than the regular braced specimen. Both specimens, however, showed a sharp drop in lateral stiffness after the first sign of brace buckling. Between ductilities of 2 and 6, there was no significant difference in lateral stiffness between the two specimens. Beyond ductility of 6, the regular braced specimen again showed superior lateral stiffness, almost remaining constant up to a ductility of 9. The overall reductions in lateral stiffness from start of loading up to ductility of 6 were 46% and 45% for the MSB specimen and regular braced specimen, respectively.

Within a specified load step, there was no significant degradation in stiffness with cycling in both specimens (Fig. 11). However, the strength of the MSB braced specimen deteriorated slightly with cycling in load steps 5, 6, and 7 as drift exceeded 2.1%. At 3.5% drift (in load step 7), the strength of this specimen dropped by about 9% at the end of that load step. For the regular braced specimen, there was no significant strength degradation with cycling up to the maximum actuator load capacity (i.e. corresponding to 3.1% specimen drift). After completing 20 load cycles to this specimen at 3.05% drift (in load step 8), its strength dropped by about 18% before the test was terminated. Fig. 14 shows the base shear-drift response for this final load step.

5.3 Energy Dissipation Characteristics of Specimens

Seismic performance of a framed structure can be measured by its energy dissipation characteristics. Energy dissipation is represented by the experimentally obtained hysteretic area, which is evaluated as the area enclosed by the base shear-deformation diagram. The cumulative hysteretic energy dissipation is a useful measure of the seismic efficiency of a structural system. In this study, both the energy dissipation per cycle, using

the first complete cycle in each load step, and the cumulative energy dissipation were presented and used in assessing individual performances and comparing the relative effectiveness of the test specimens. The cumulative dissipated hysteretic energy was normalized at each cycle by the product of specimen yield base shear and yield displacement, $V_y\Delta_y$, to eliminate the effect of varying yield loads and displacements. For both specimens, there was no significant amount of energy dissipation within the elastic range of loading. Appreciable energy was dissipated after the elastic cycles, and increased in the following cycles.

Fig. 15 shows the variation in energy dissipation per cycle, using the first complete cycle at each load step, versus peak drift and maximum displacement ductility reached during that same load cycle. It can be observed that up to maximum displacement ductility of 2, both the MSB and the regular braced specimens exhibited similar energy dissipation per cycle. Beyond this ductility level, the MSB specimen showed superior energy dissipation per cycle in each of the load steps until end of the test. At the maximum displacement ductility of 4, for example, the energy dissipated per cycle by the regular braced specimen was about 77% that by the MSB specimen. For the regular braced specimen, there was no significant deterioration of dissipated energy with cycling in load step 8 (i.e. at 3.05% drift) before the end of the test. Energy dissipated in the first cycle of this load step reduced by only about 1.5% at the end of the 18^{th} cycle of that same load step.

Fig. 16 shows the variation of normalized cumulative energy dissipation with cumulative number of cycles and maximum displacement ductility of the test specimens. Clearly, both specimens dissipated similar amount of normalized cumulative energies. The majority of dissipated energy in the MSB braced specimen was the result of a combination

of bending deformation in the tube column segment between the top flange of the ceiling beam and the bottom flange of the floor beam, and tension yielding and inelastic buckling of the bracing members. For the regular braced specimen, energy was mainly dissipated through tension yielding and inelastic buckling of the HSS bracing members.

5.4 Force Distribution Pattern

The measured strain in member sections of the test specimens can be closely linked to the distribution of applied lateral load in these members. Figs. 17 and 18 show the strain evolution measured at a selected section of similar brace members (a mid-section of upper half-side of a brace member, labeled “e” in Fig. 6) of the specimens with cyclic loading at load steps 2 (elastic load cycles) and 4 (inelastic load cycles with maximum displacement ductility of 4), respectively. The slope of the line joining the peaks of the strain distribution curves is used here as indicative of the distribution of applied shear force at a specified deformation level in the two specimens. This is used to obtain a rough estimate of the force distribution pattern in the selected brace member of the two specimens.

In the elastic load cycle (i.e. step 2), the slopes of the peak-to-peak lines from the two specimens were found to be similar, indicating that the distribution of the applied lateral load within the selected brace member section is of similar pattern. The difference in configuration of the test specimens appears not to have any effect on this force distribution. In the inelastic load cycle (i.e. load step 4), the MSB braced specimen appear to yield greater slope than the regular braced specimen (9.1 micro strain per kN compared to 8.7 micro strain per kN). This implies that, the brace member of the MSB specimen at the selected brace section experienced greater strain than that of the regular specimen under the

same load level. In other words, to achieve the same level of strain (deformation) in the member section selected, a greater amount of shear needs to be applied to the regular specimen than the MSB specimen.

Strain gauge readings at several sections of the various members of the specimens were extracted at a number of load levels belonging to both elastic and inelastic ranges of response and in both directions of loading. The force distribution in the two specimens was compared for same load levels in similar cycle numbers within similar load steps. Also, the comparison was made for a similar load level applied at different load steps and for a similar load level applied in opposite directions of the MSB specimen.

Fig. 19 can be used to explain the force distribution pattern in both the MSB and regular braced specimens. Buckling of brace sections was identified by observing high discrepancies in the magnitude of forces, and the magnitude of moments evaluated for these sections in-plane and out-of-plane. Table 2 provides the ratios of calculated normal forces in members of the test specimens to the applied lateral load, P. Negative signs in this table represent a reverse of force sense from that shown in Fig. 19. The calculated moments in the various members were found to be negligible compared to the normal forces, and have therefore not been included in the discussions below.

At load levels within the elastic response range (load step 2), there is only a small difference in magnitude of distributed loads in the columns and braces between the two specimens. However, the overall mechanisms of load transfer vary due to difference in configuration. For the regular braced specimen (Fig. 19b), similar force levels are transmitted through joints x1 and x2, with a difference of only about 2% of the applied lateral force. The top floor beam thus carries almost half of the applied force along its

longitudinal plane. Consequently, the columns and braces develop the induced forces. This force distribution pattern is due to the near truss action exhibited by the frame. For the MSB specimen, unequal forces are transmitted through joints x3 and x4. This is due to the welding detail at the vertical module connection. There is partial welding between the columns and the top floor beam, which leaves interior sides of the joints without weld. Thus, in the direction of loading, the leading joint allows some rotation to occur. The trailing joint, on the other hand, develops some moments. The ceiling beam aids redistribution of these unbalanced forces by developing a normal force with the same sense of direction as the floor beam. Joints x5 and x6 thus transmit an equal amount of force, and consequently the brace members and column members develop equal amount of forces between themselves.

In the inelastic range of response of the regular specimen (load steps 3, 5, 6), buckling of compression brace member section results in the reduction of distributed force through the end joint of this brace member and an increase in the force through the end joint of the tension brace. This results in an unequal force distribution in bracing members, and also in column members, as shown in Table 2. For the MSB specimen, joints x3 and x4 experience different degrees of transmitted force as explained above. Once buckling of the compression brace occurs, the ceiling beam member helps in redistributing these forces allowing greater force levels through the end joint of the tension brace. If the direction of loading is reversed, a similar behaviour is observed in the opposite direction. At high lateral loads, however, the transmission of compression forces across brace intersection in the non-continuous brace member is significantly affected by buckling and this complicates the overall transfer mechanism.

5.5 Analytical Prediction of MSB Specimen behavior

The behavior of the MSB test specimen was predicted analytically using a two-dimensional model. A basic two-dimensional centerline model of the frame specimen was used with floor and ceiling beams, columns and braces extending from centerline to centerline. A bilinear material model for steel was employed, using the experimentally obtained material properties. An inelastic steel beam-column frame element was used to represent column members. A one component beam element was used for all beam representations. The inelastic behavior of both the beam and the beam-column elements follows the concept of the Giberson one-component model [21], which has a plastic hinge possible at one or both ends of the elastic central length of the member. The Remennikov Steel Brace model [22] was used to represent bracing members. This hysteresis model represents the out-of-plane buckling of the steel brace member but essentially captures the inelastic behaviour under alternate axial tension and compression. This member only permits this hysteresis in the axial component; it is generally assumed to be bi-linear in flexure.

All beam-column joints in the MSB specimen model were assumed rigid to represent the directly welded connection between these members. Rigid end blocks were provided at each end of the frame members to capture the rigidity of connection regions. A truss action of the bracing members was activated by allowing both ends to be pinned internally to the joints. This was to simulate the assumed pin-ended behaviour of bracing members. The proposed model of the vertical connection of separate units, between columns of a lower unit and the top floor beam (or columns) of an upper unit, described in section 3.4.2 above was adopted in this prediction analysis.

Fig. 20 shows a comparison between the experimentally and theoretically obtained load-displacement curves of the MSB braced specimen. It can be observed that the theoretical model provided a fairly good prediction up to a displacement of 36 mm (corresponding to 2.8% drift), beyond which it experienced numerical instability. Prior to termination of the analysis, bracing members experienced repeated inelastic deformations in cyclic tension beyond yield and compression into the post-buckling range. The columns, including column segments between the bottom flange of the floor beam and top flange of the ceiling beam, also experienced repeated cycles of bending deformation before the end of the analysis.

6.0 Summary and Conclusions

This study has evaluated the hysteretic characteristics of modular steel building (MSB) braced frame under repeated cyclic loading. The stiffness, ductility, cumulative hysteretic energy dissipation capacity, and force distribution pattern were assessed. The behavior of the MSB specimen was predicted analytically to validate a proposed modeling technique. The design and construction of the test specimen accounted for the building's specific detailing requirements. A regular concentrically braced frame with similar physical characteristics, such as clear height and member proportions, was also tested to compare behavior. The results of the tests indicate some similarities as well as some differences in behavior of the two test specimens. The differences in behavior particularly suggested that for improved performance of MSB braced frames, the detailing requirements of the system, such as the vertical connection of separate units, need to be incorporated in their design.

This would allow the frame members to develop their full capacity as expected from the design philosophy. The observations made in the tests have been summarized below.

1. Both the MSB and regular braced specimens showed stable and ductile behavior up to very high drift levels. The MSB specimen reached a ductility of 10 at 3.5% drift and the regular specimen reached a ductility of 9 at 3.1% drift at a load level equal to the load capacity of the actuator. The regular specimen further sustained 20 more cycle at 3.05% drift before the test was terminated.
2. The hystereses of both specimens were fairly symmetrical with some degree of pinching, especially in the regular specimen. For the regular specimen, the first sign of nonlinearity occurred as a result of buckling in a brace member while in the MSB specimen, flexural response due to column yielding caused the initial nonlinearity.
3. The regular braced specimen was found to be slightly superior in terms of lateral stiffness at low ductility (below 2) and at high ductility (above 6). Between these ductilities, both frame specimens showed similar stiffness levels. For both specimens, initial stiffness degraded by about 45% at a ductility level of 6.
4. Within each load step in the regular braced specimen, there was no significant strength and stiffness degradation with cycling. The MSB specimen also showed no significant stiffness degradation but only slight reduction (less than 10% at 3.5% drift) in strength with cycling beyond a 2.1% drift.
5. For the MSB specimen, the test was terminated after a high level of ductility was reached. In this stage of loading, severe bending deformation was observed for the column segment between the top flange of the ceiling beam and the bottom flange of the floor beam. The brace members in this specimen did not suffer severe

deformation. For the regular braced specimen, the test was terminated after several inelastic cycles at sufficiently high ductility level. Prior to this point, a lower half side of a brace member experienced severe out-of plane buckling at its mid-section.

6. Both specimens dissipated significant and similar amount of cumulative energies. Both specimens also exhibited similar energy dissipation per cycle up to ductility of 2. Beyond this ductility level, the MSB specimen appeared to show superior energy dissipation per cycle in each of the load steps until failure.
7. Significantly different force distribution patterns were observed in the two test specimens. At the same load level corresponding to the same number of cycles in a similar load step, the load transfer mechanism in the MSB specimen produced force distribution that are different from the regular braced specimen because of the presence of the ceiling beam and the unique vertical connection of separate modules.
8. The proposed analytical modeling technique is capable of predicting the seismic behavior of MSB braced frames up to high drift levels beyond traditional design requirements.

Acknowledgements

This research was funded by the National Sciences and Engineering Research Council of Canada (NSERC) and The University of Western Ontario.

References

[1] Osteraas J, Krawinkler H. The Mexico earthquake of September 19, 1985 – behavior of steel buildings. Earthquake Spectra 1989;5(1):51-88.

[2] Tremblay R, Timler P, Bruneau M, Filiatrault A. Performance of steel structures during the January 17, 1994 Northridge earthquake. Can J of Civil Eng. 1995;22(2):338-60.

[3] Tremblay R, Bruneau M, Nakashima M, Prion HGL, Filiatrault A, DeVall R. Seismic design of steel buildings: Lessons from the 1995 Hyogo-ken Nanbu earthquake. Can J of Civil Eng. 1996;23(3):727-56.

[4] Jain AK, Goel SC. Hysteresis models for steel members subjected to cyclic buckling or cyclic end moments and buckling – User's guide for DRAIN-2D: EL9 and EL10. Report UMEE 78R6 1978, Department of Civil Eng., Univ. of Michigan, Ann Arbour, MI, USA.

[5] Ikeda K, Mahin SA. A refined physical theory model for predicting the seismic behavior of braced steel frames. Report no. UCB/EERC-84/12 1984, Berkeley, CA.

[6] Tremblay R. Inelastic seismic response of steel bracing members. J of Constructional Steel Research 2002;58:665-701.

[7] Tremblay R, Archambault MH, Filiatrault A. Seismic response of concentrically braced steel frames made with rectangular hollow bracing members. Journal of Structural Engineering, ASCE 2003;129(12):1626-36.

[8] CSA. Handbook of Steel Construction, 7th Edition, Willowdale ON: Canadian Institute of Steel Construction, 2001.

[9] AISC. Seismic provisions for structural steel buildings, IL: American Institute of Steel Construction, 2002.

[10] Annan CD, Youssef MA, El-Naggar MH. Analytical investigation of semi-rigid floor beams connection in modular steel structures. 33rd Annual general conference of the Canadian Society for Civil Engineering, Toronto 2005; GC-352.

[11] Annan CD, Youssef MA, El-Naggar MH. Seismic performance of modular steel braced frames. Proc. of the Ninth Can Conf on Earthquake Eng, Ottawa, 2007.

[12] Annan CD, Youssef MA, El-Naggar MH. Seismic overstrength in braced frames of Modular Steel Buildings. Journal of Earthquake Engineering 2009;13(1):1-21.

[13] Annan CD, Youssef MA, El-Naggar MH. Effect of directly welded stringer-to-beam connections on the analysis and design of modular steel building floors. Advances in Structural Engineering, Accepted in October 2008.

[14] NBCC. National Building Code of Canada, Institute for Research in Construction, Ottawa ON: National Research Council of Canada 2005.

[15] Yoo J-H, Roeder CW, Lehman DE. Analytical performance simulation of special concentrically braced frames. Journal of Structural Engineering 2008;134(6): 881-889.

[16] ASTM. Standard test methods and definitions for mechanical testing of steel products, Philadelphia PA: American Society for Testing and Materials 2002.

[17] Izzuddin BA. Nonlinear dynamic analysis of framed structures. PhD Thesis, Imperial College, University of London 1991, London.

[18] Rahgozar MA, Humar JL. Accounting for overstrength in seismic design of steel structures. Canadian Journal of Civil Engineering *1998;*25:1–15.

[19] FEMA. Pre-standard and Commentary for the seismic rehabilitation of buildings. Prepared by the American Society of Civil Engineers for the Federal Emergency Management Agency 2000, Washington, D.C, (FEMA Publication No. 356).

[20] ATC. ATC-24/Guidelines for cyclic seismic testing of components of steel structures, Redwood City, CA: Applied Technology Council, 1992.

[21] Sharpe RD. The seismic response of inelastic structures. Ph.D Thesis, Department of Civil Engineering, University of Cantebury, 1974.

[22] Remennikov A, Walpole W. Analytical prediction of seismic behaviour for concentrically-braced steel systems. Earthquake Engineering and Structural Dynamics 1997;26:859-74.

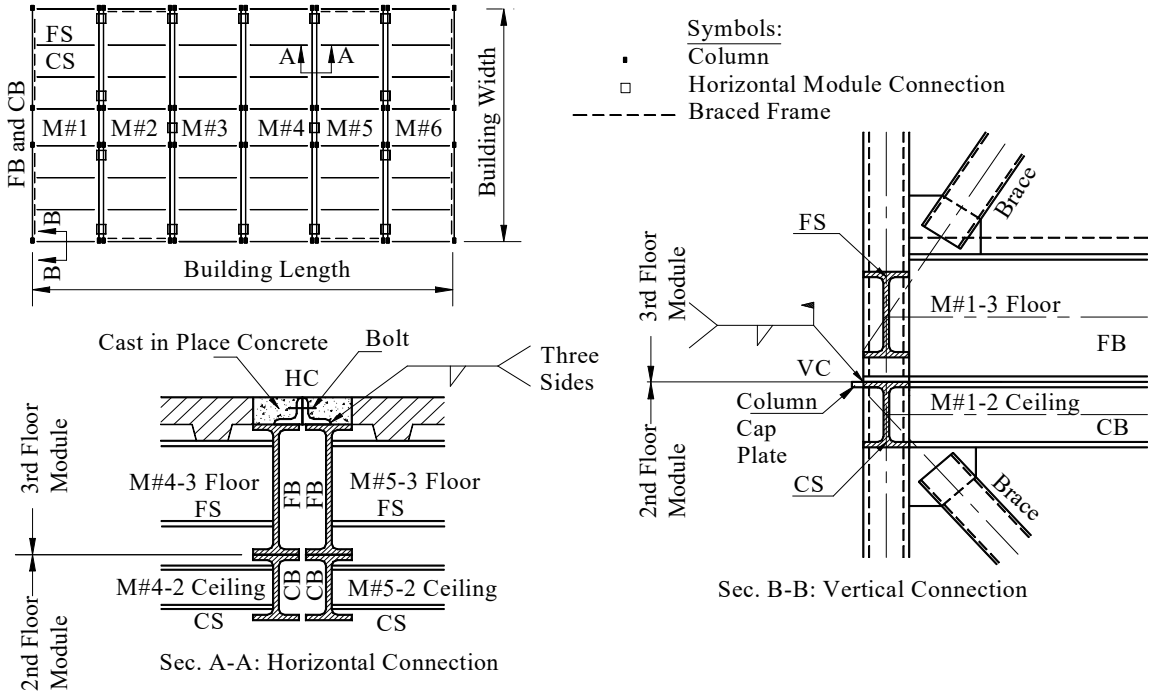

Fig. 1. A typical plan and sections of a modular steel building

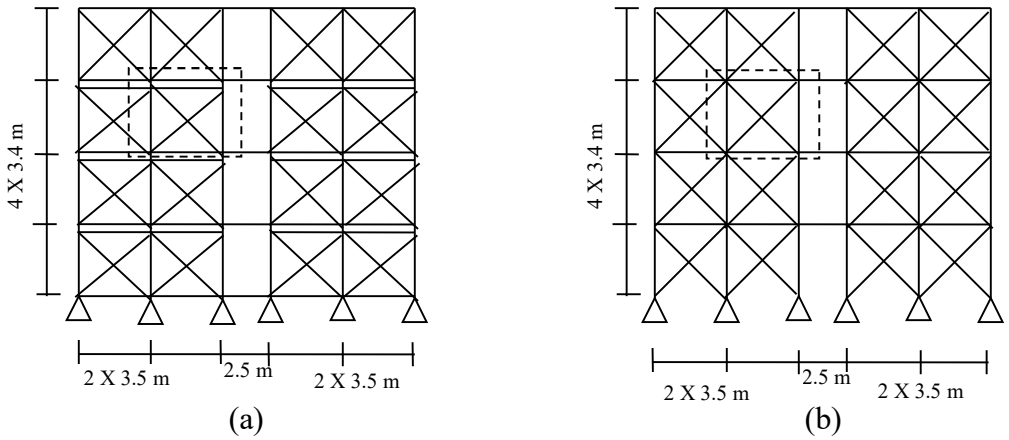

Fig. 2. Four-storey braced frames for design of test specimens (a) MSB frame (b) Regular frame

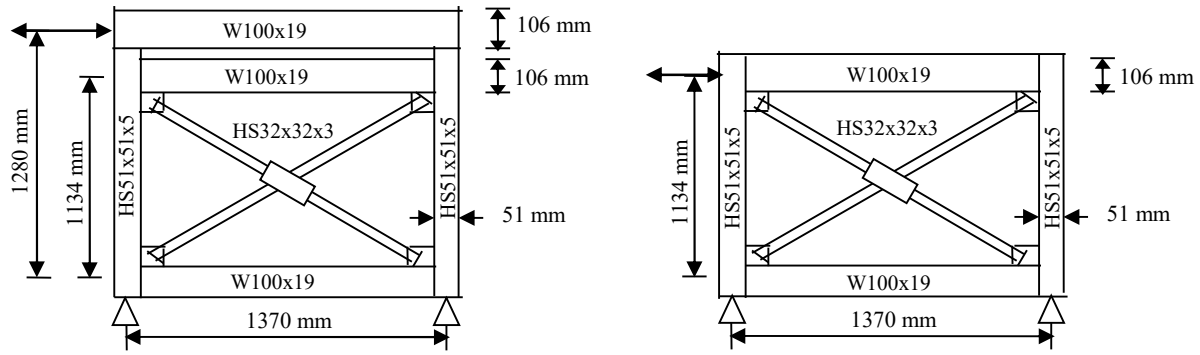

Fig. 3. Dimensions of test specimens (a) MSB braced frame (b) Regular braced frame

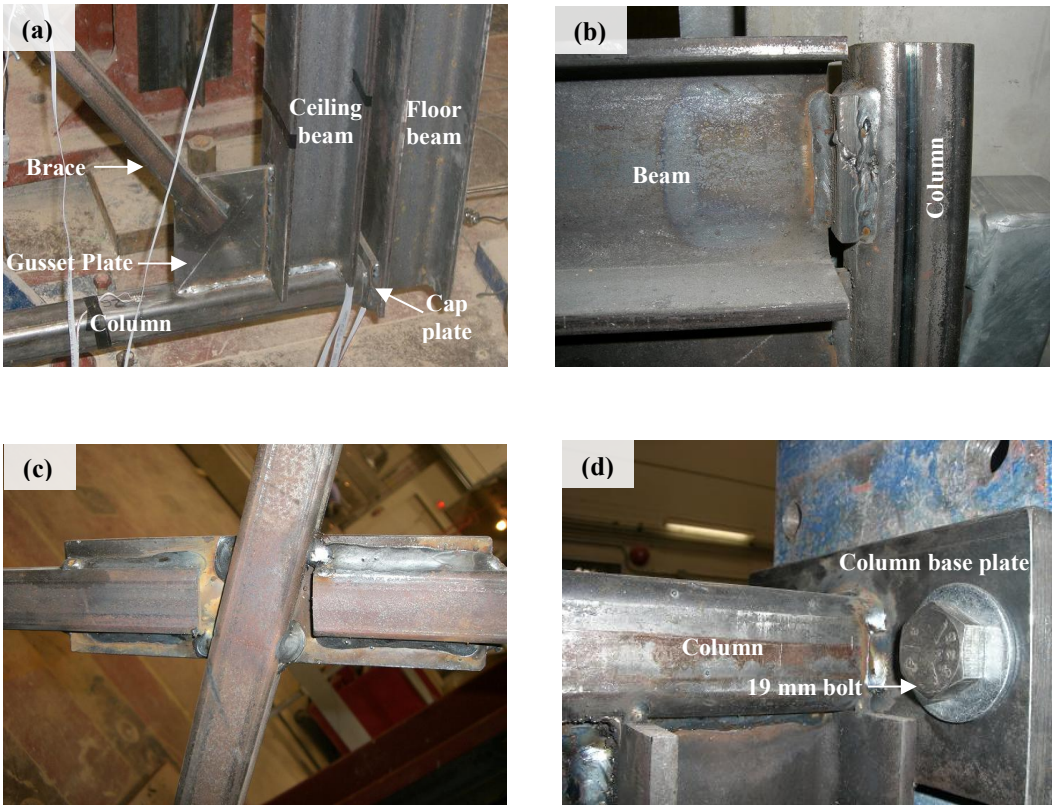

Fig. 4. (a) Some member and connection details in MSB specimen (b) Beam-to-column connection in Regular specimen (c) Brace intersection detail of specimens (d) Column base plate connection to reaction frame

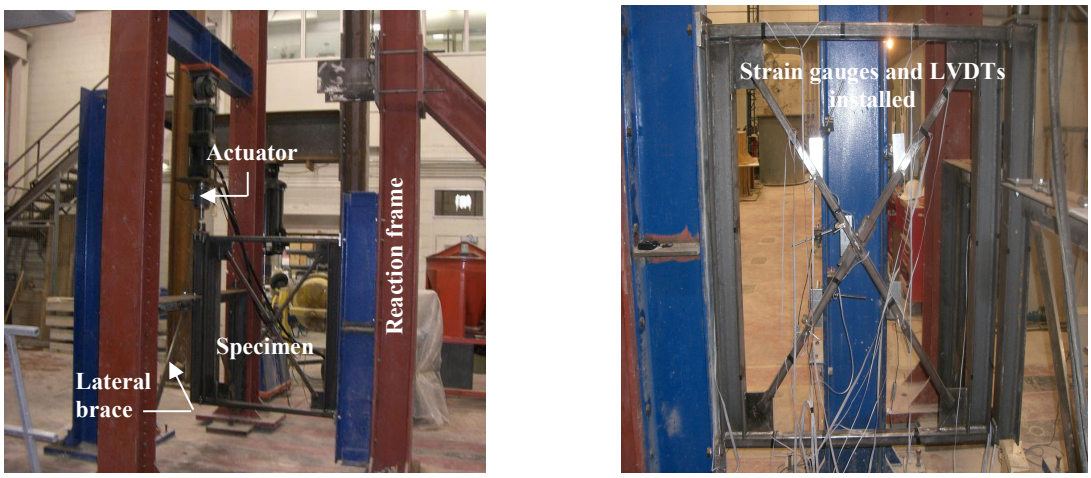

Fig. 5. Overall view of test setup

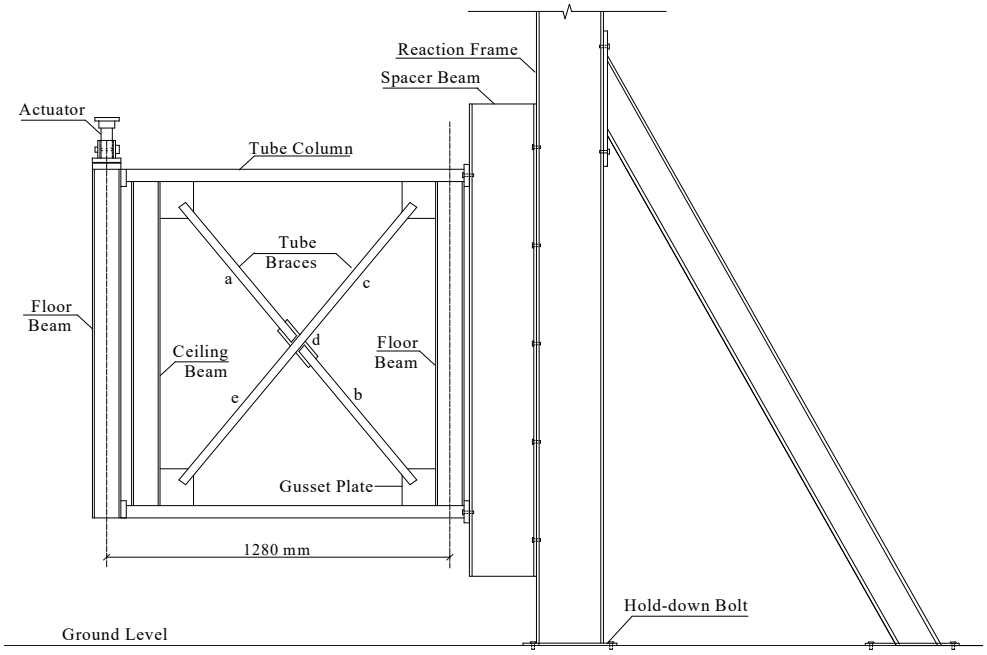

Fig. 6. Schematic representation of test setup

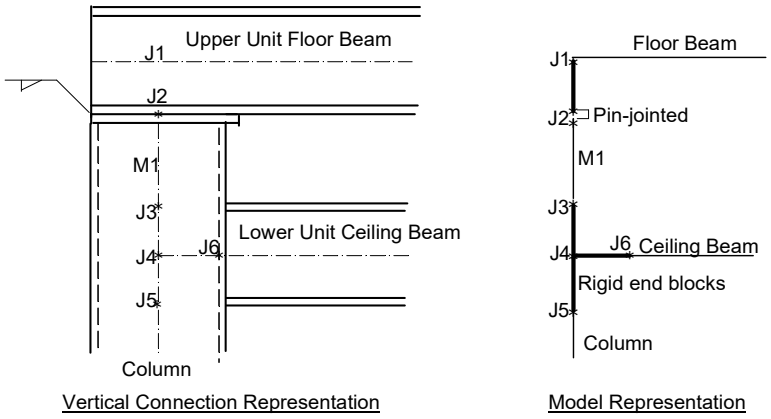

Fig. 7. Model of vertical connection of units of MSB specimen

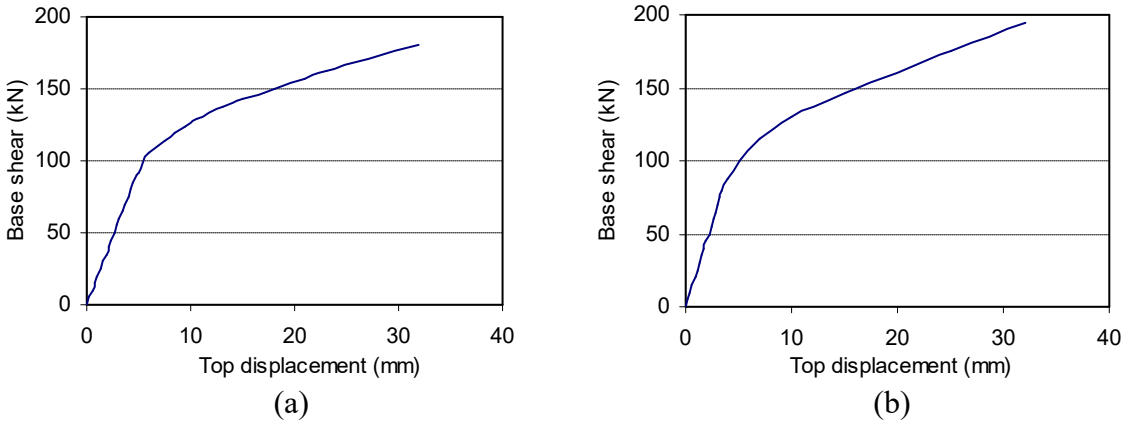

Fig. 8. Pushover curves for (a) MSB braced specimen (b) Regular braced specimen

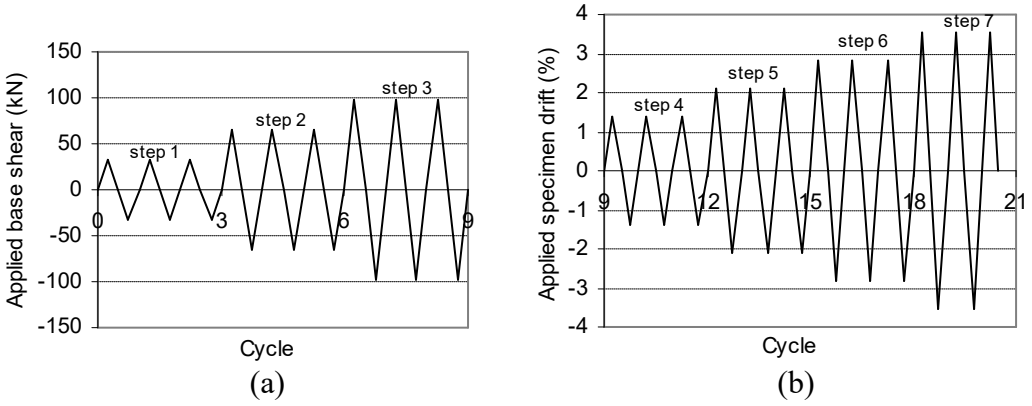

Fig. 9. Loading history for MSB braced specimen (a) elastic cycles (b) inelastic cycles

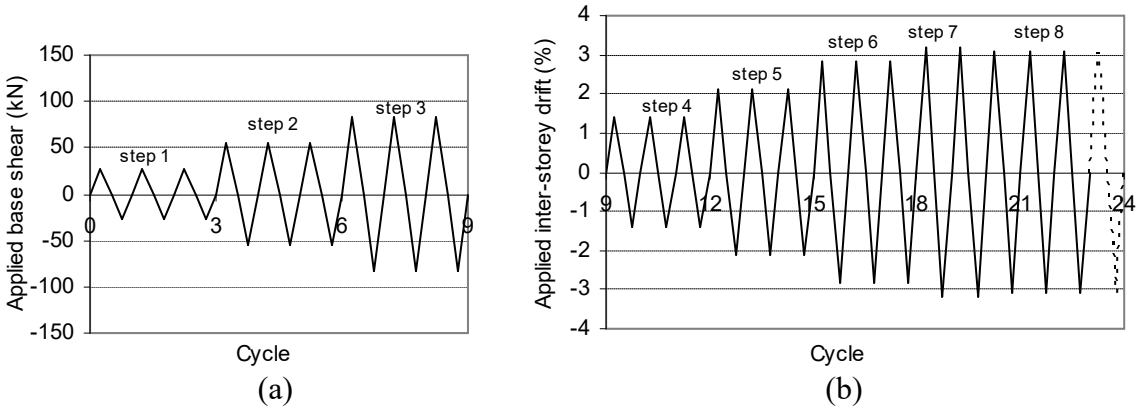

Fig. 10. Loading history for Regular braced specimen (a) elastic cycles (b) inelastic cycles

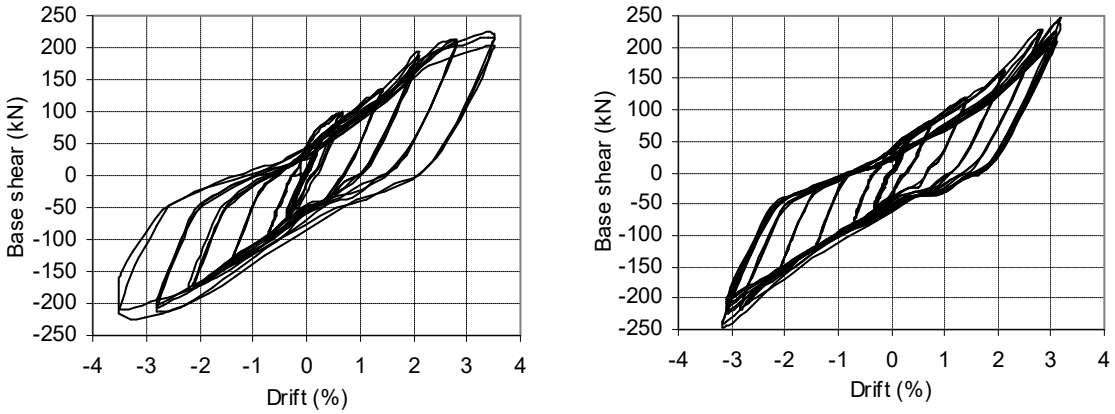

Fig. 11. Base shear versus drift hysteretic response (a) MSB specimen (b) regular braced specimen

Fig. 12. (a) Column bending deformation in MSB braced specimen (b) Brace out-of-plane deformation in regular braced specimen

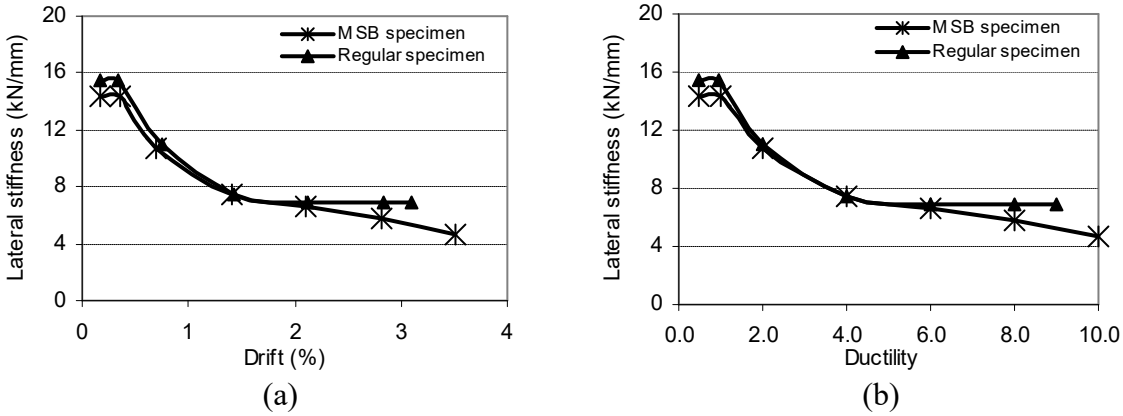

Fig. 13. Variations of lateral stiffness with (a) peak drift (b) maximum ductility

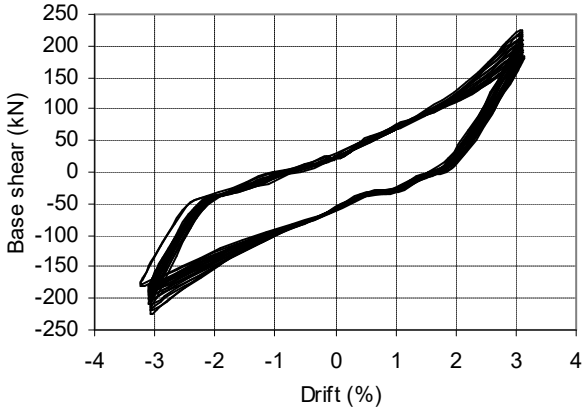

Fig. 14. Base shear versus drift relationship for regular braced specimen at 3.05% drift

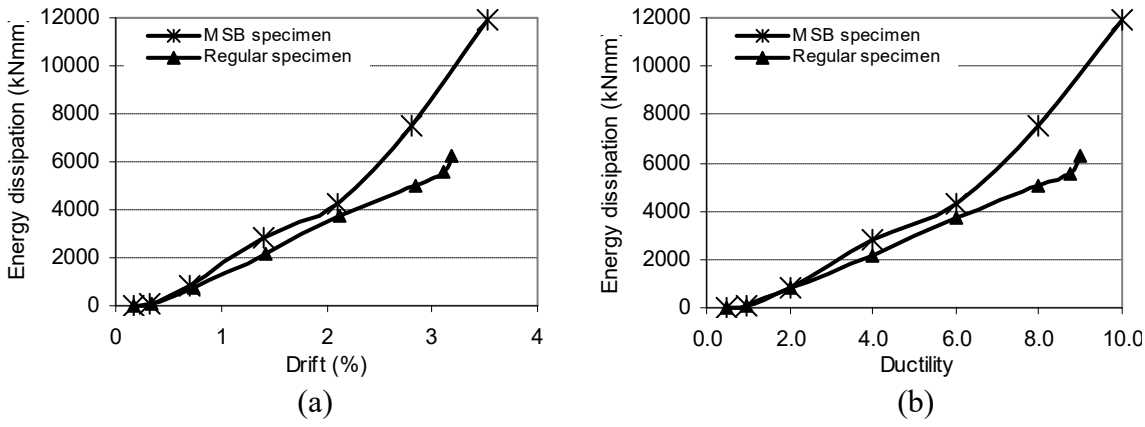

Fig. 15. Energy dissipation per cycle versus (a) peak drift (b) maximum ductility

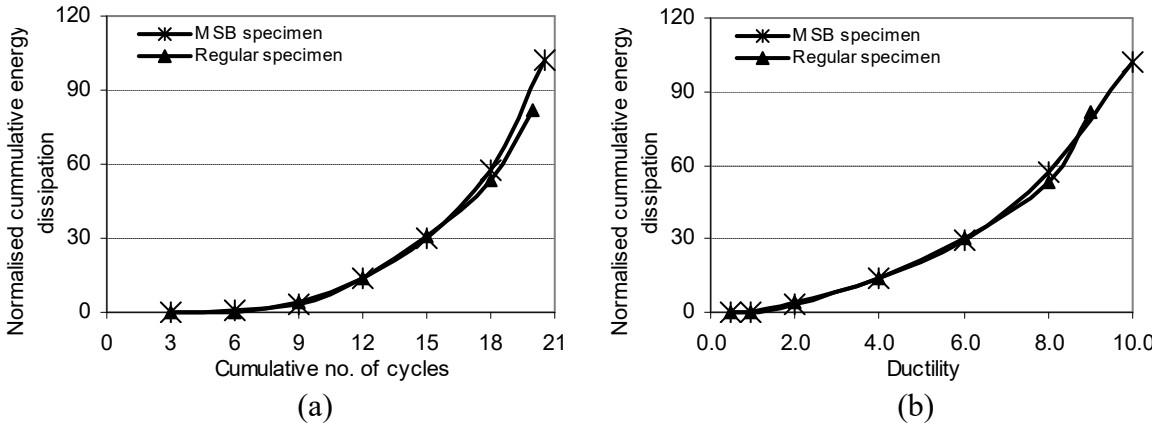

Fig. 16. Comparison of normalized cumulative energy dissipation for specimens

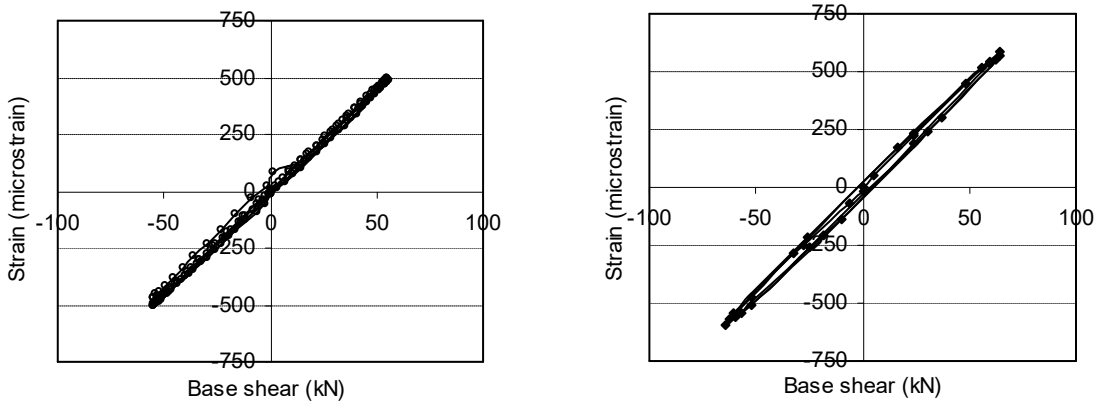

Fig. 17. Strain evolution in a brace member section at load step 2 (a) regular specimen (b) MSB specimen

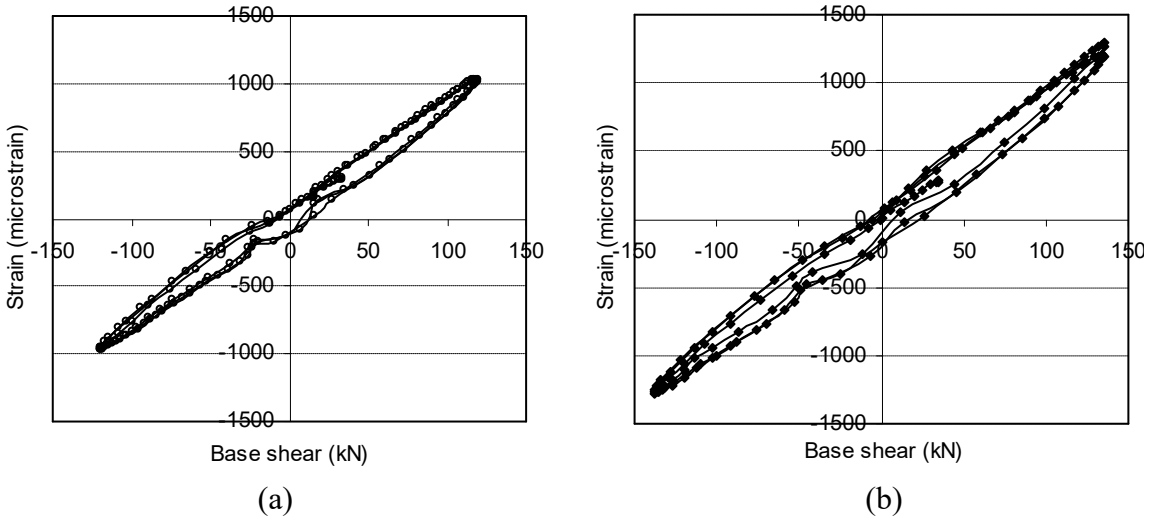

Fig. 18. Strain evolution in a brace member section at load step 4 (a) regular specimen (b) MSB specimen

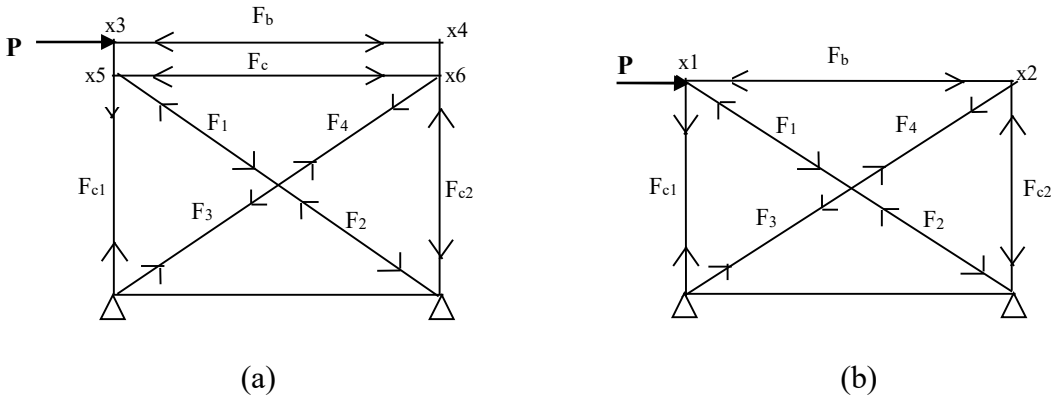

Fig. 19. Force distribution in members of (a) MSB specimen (b) regular braced specimen

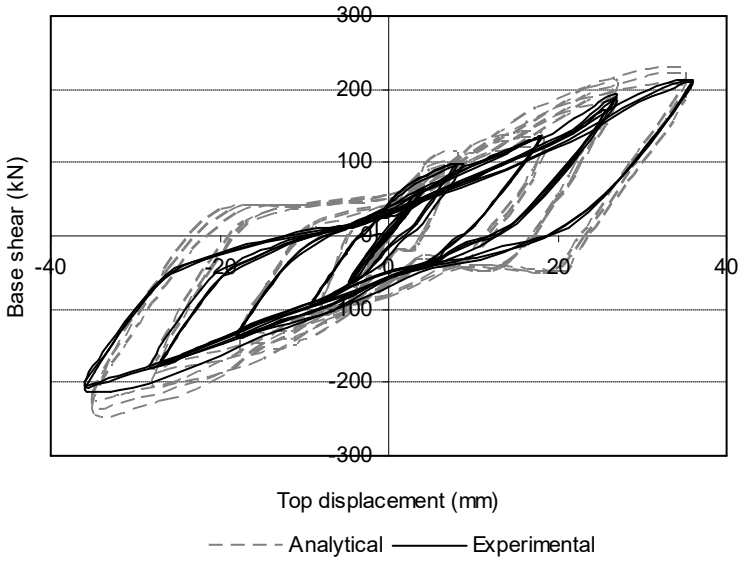

Fig. 20. Comparison of experimental and analytical load-displacement curves of MSB braced specimen

Table 1. Ductility levels reached by specimens at different cycles

Step	MSB braced specimen		Regular braced specimen	
	Cycle number	Normalised peak deformation (Δ/Δy)	Cycle number	Normalised peak deformation (Δ/Δy)
1	1 - 3	0.49	1 - 3	0.48
2	4 - 6	0.97	4 - 6	0.95
3	7 - 9	2.00	7 - 9	2.00
4	10 - 12	4.00	10 - 12	4.00
5	13 - 15	6.00	13 - 15	6.00
6	16 - 18	8.00	16 - 18	8.00
7	19 - 20.5	10.00	19 - 20	9.00
8			21 - 40	8.75

Table 2. Force distribution ratios in members of braced specimens

Specimen	Load step	P (kN)	F_1	F_2	F_3	F_4	F_{c1}	F_{c2}	F_b	F_c
MSB	2	-45.1	-0.65	-0.64	-0.65	-0.65	-0.45	-0.45	-0.36	-0.14
Regular	2	-45.3	-0.66	-0.66	-0.63	-0.63	-0.43	-0.40	-0.49	
MSB	2	40.8	0.65	0.64	0.64	0.64	0.46	0.45	0.35	0.15
Regular	2	40.5	0.67	0.66	0.64	0.64	0.44	0.42	0.49	
MSB	3	82.5	0.59	0.58	0.71	0.71	0.42	0.50	0.36	0.19
Regular	3	81.8	0.61	0.60	0.69	0.69	0.40	0.45	0.54	
MSB	5	-193.7	-0.76	-0.75	-0.52	-0.53	-0.53	-0.38	-0.37	-0.05
MSB	6	-193.7	-0.78	-0.76	-0.50	-0.51	-0.54	-0.37	-0.36	-0.04
MSB	6	-213.4	-0.78	-0.75	-0.49	-0.51	-0.55	-0.37	-0.36	-0.04
MSB	6	213.3	0.48	0.43	0.80	0.78	0.35	0.56	0.36	0.27